

Copper nanoparticle ensembles for selective electroreduction of CO₂ to C₂–C₃ products

Dohyung Kim^{a,b,c}, Christopher S. Kley^d, Yifan Li^{b,c,d}, and Peidong Yang^{a,b,c,d,1}

^aDepartment of Materials Science and Engineering, University of California, Berkeley, CA 94720; ^bChemical Sciences Division, Lawrence Berkeley National Laboratory, Berkeley, CA 94720; ^cKavli Energy NanoScience Institute, Berkeley, CA 94720; and ^dDepartment of Chemistry, University of California, Berkeley, CA 94720

Contributed by Peidong Yang, August 15, 2017 (sent for review June 27, 2017; reviewed by Matthew Kanan and Kyung Byung Yoon)

Direct conversion of carbon dioxide to multicarbon products remains as a grand challenge in electrochemical CO₂ reduction. Various forms of oxidized copper have been demonstrated as electrocatalysts that still require large overpotentials. Here, we show that an ensemble of Cu nanoparticles (NPs) enables selective formation of C₂–C₃ products at low overpotentials. Densely packed Cu NP ensembles underwent structural transformation during electrolysis into electrocatalytically active cube-like particles intermixed with smaller nanoparticles. Ethylene, ethanol, and *n*-propanol are the major C₂–C₃ products with onset potential at –0.53 V (vs. reversible hydrogen electrode, RHE) and C₂–C₃ faradaic efficiency (FE) reaching 50% at only –0.75 V. Thus, the catalyst exhibits selective generation of C₂–C₃ hydrocarbons and oxygenates at considerably lowered overpotentials in neutral pH aqueous media. In addition, this approach suggests new opportunities in realizing multicarbon product formation from CO₂, where the majority of efforts has been to use oxidized copper-based materials. Robust catalytic performance is demonstrated by 10 h of stable operation with C₂–C₃ current density 10 mA/cm² (at –0.75 V), rendering it attractive for solar-to-fuel applications. Tafel analysis suggests reductive CO coupling as a rate determining step for C₂ products, while *n*-propanol (C₃) production seems to have a discrete pathway.

heterogeneous catalysis | electrocatalysis | CO₂ reduction | copper nanoparticles | in situ structural transformation

With rising concerns about the anthropogenic impacts of current trends in energy use, as well as the prospect of continuing these trends to meet future needs (1), we are at a stage where revolutionary change to our energy paradigm is a must. Various methods for effectively using solar energy are being developed to power and support the global population (2–4). Among them, artificial photosynthesis is considered vital to meeting our goal toward long-term global sustainability (5). The successful introduction of artificial photosynthesis technology will highly depend on the development of every functional component essential to the efficient operation of the overall system.

As energy from sunlight eventually ends up in chemical bonds by the photocatalytic or electrocatalytic component, development of an effective catalytic material to facilitate the conversion process becomes important. Over the past several decades, the focus has been on using water as the starting substrate and converting it to hydrogen gas (6). More recently, carbon dioxide has been considered as a promising substrate, and many efforts have been underway to find efficient electrocatalysts that can selectively operate for reducing CO₂ in aqueous solutions against the competing hydrogen evolution (7–16). However, major progress has been limited to two-electron reduced products of CO and formate. Still, the formation of multicarbon products involving multiple proton and electron transfers remains as one of the biggest scientific challenges to be addressed.

Starting from the idea that element copper is a key component to forming multicarbon products (17, 18), there have been

various studies so far where formation of products such as C₂H₄, C₂H₆, and C₂H₅OH has been observed often with the requirement of large overpotentials (potential applied ≤ –1 V vs. RHE) (19–35). These methods mostly rely on reducing certain forms of oxidized copper (19–25, 27–30, 32–34) (either oxides or halides) and even this approach has been extended to reduce carbon monoxide instead (36), a common intermediate for CO₂ reduction, to circumvent difficulties associated with C–C coupling starting from CO₂. Furthermore, to instead create a favorable environment for multicarbon product formation, there have been attempts to use gas-diffusion electrodes with alkaline electrolytes (37). It would certainly be desirable to discover an electrocatalyst that can directly reduce CO₂ to multicarbon products with high selectivity and energy efficiency (i.e., minimal energy loss from low overpotentials).

Here, we show that an ensemble of densely packed copper nanoparticles (NPs) could enable selective conversion of CO₂ to multicarbon products, while significantly suppressing C₁ formation. Catalytically active cube-like structures, capable of forming ethylene, ethanol, and *n*-propanol, are formed during electrolysis by the structural transformation of the Cu NP ensemble. These structures can selectively generate C₂ and C₃ products together at low overpotentials in neutral pH aqueous media, illustrating the importance of in situ structural evolution in CO₂ electrocatalysis. We also find that the catalyst support plays an important role for high multicarbon selectivity. This work suggests an alternative route to development of catalysts for multicarbon products and understanding of their formation, where the field has been heavily reliant on using oxidized copper as starting materials.

Significance

Electrochemical conversion of CO₂ to carbon-based products, which can be used directly as fuels or indirectly as fuel precursors, is suggested as one of the promising solutions for sustainability. Not only does this process allow using renewables such as solar electricity as energy input, but CO₂ emitted from the consumption process can be recycled back into fuels. The success of this technology depends on the value added to the product that forms from CO₂, and therefore it is important to facilitate multicarbon product generation. This work presents a copper-based catalyst, formed in situ from an ensemble of nanoparticles, that is able to selectively generate C₂–C₃ products at low overpotentials with good stability, where their efficient formation has been difficult to achieve.

Author contributions: D.K. and P.Y. designed research; D.K., C.S.K., and Y.L. performed research; D.K., C.S.K., and Y.L. analyzed data; and D.K. and P.Y. wrote the paper.

Reviewers: M.K., Stanford University; and K.B.Y., Sogang University.

Conflict of interest statement: Provisional patent application filed based on the technology described in this work.

¹To whom correspondence should be addressed. Email: p_yang@berkeley.edu.

This article contains supporting information online at www.pnas.org/lookup/suppl/doi:10.1073/pnas.1711493114/-DCSupplemental.

Results and Discussion

Monodisperse Cu NPs (size 6.7 nm) prepared (*SI Appendix, Fig. S1*) were directly deposited onto carbon paper support ($1 \text{ cm}^2_{\text{geo}}$) to form densely packed NP ensembles. Cu NP loading was systematically increased (*SI Appendix, Table S1*) starting from the lowest loading of $\sim 2 \mu\text{g}$ of Cu ($\times 1$). Number density of NPs was determined based on the estimated surface area of the carbon paper support (24, 26) (*SI Appendix, Fig. S2*), which was at $\sim 5.9 \text{ cm}^2_{\text{real}}/\text{cm}^2_{\text{geo}}$ (roughness factor ~ 5.9). Most of the NPs are isolated at the lowest loading condition, and increased loadings

resulted in densely packed arrangements of Cu NPs (Fig. 1A). In the case of $\times 22.5$ loading, the surface was mostly covered with closely packed Cu NPs (*SI Appendix, Fig. S3*).

Cu NP ensembles with varied loading densities were tested for their electrocatalytic CO_2 reduction activity, under identical conditions of 0.1 M KHCO_3 at 1 atm CO_2 . From product analysis (*SI Appendix, Fig. S4*), we found that increased loadings resulted in a drastic rise of the $\text{C}_2\text{--C}_3$ faradaic efficiency (FE) (Fig. 1B and *SI Appendix, Fig. S5* and Table S2). This trend is consistent with the observed loss of C_1 products, indicating that carbon-based intermediates could be effectively coupled to yield

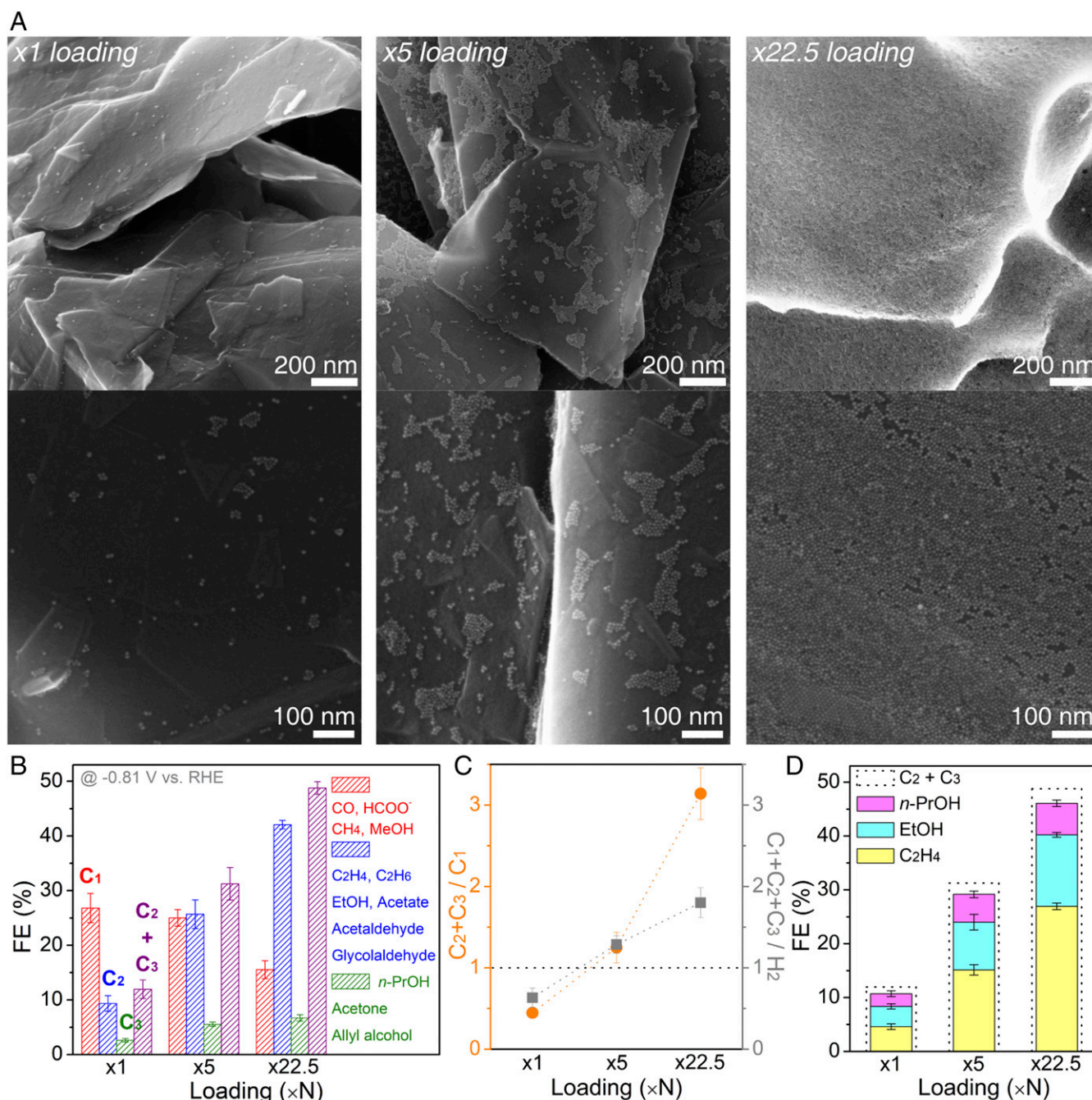


Fig. 1. Varied density of Cu NP ensembles and their electrocatalytic activity. (A) SEM images of Cu NPs loaded on carbon-paper support at $\times 1$ loading, $\times 5$ loading, and $\times 22.5$ loading. (B) FEs (%) for C_1 , C_2 , and C_3 products. (C) Relative ratio of the FEs. (D) Ethylene, ethanol, and n -propanol FE with the dotted line showing the overall $\text{C}_2\text{--C}_3$ FE. Activity measured at -0.81 V vs. RHE , using 0.1 M KHCO_3 saturated under 1 atm CO_2 . Error bars shown in B–D are 1 SD from three independent measurements.

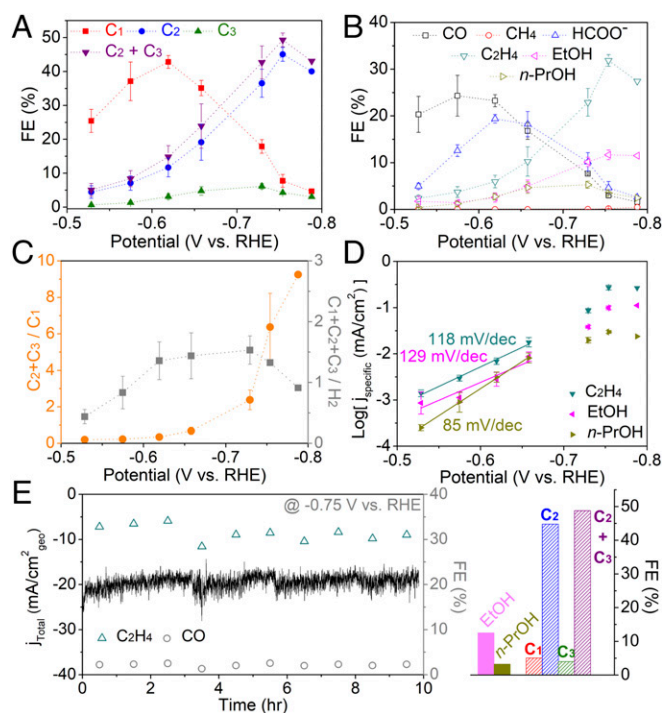
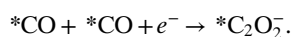


Fig. 4. Electrocatalytic behavior of trans-CuEn 2 ($\times 32.5$ loading in 0.1 M CsHCO₃). (A) FE of C₁, C₂, and C₃ products at various potentials. (B) FE of major products at various potentials. (C) Relative ratio of the FE. (D) Logarithmic specific current density (corrected by the real surface area of the catalyst) plots for C₂H₄, EtOH, and *n*-PrOH. Electrochemical tests were conducted in 0.1 M CsHCO₃ solution at 1 atm CO₂. Error bars shown are 1 SD from three independent measurements. (E) Long-term electrolysis at -0.75 V vs. RHE with gas products measured every hour. Column graph on the right shows FE of EtOH and *n*-PrOH measured after electrolysis and C₁, C₂, and C₃ product FEs for the overall run.

C₂H₄ and EtOH start forming in the potential region where CO evolution is dominant and increase while CO diminishes (Figs. 3B and 4B), suggesting that formation of these C₂ products is essentially limited by the coupling of major C₁ intermediates. It has been also shown that higher coverages of *CO can be expected in the region where CO formation is majorly observed (48). Therefore, with a slope close to 120 mV/dec suggesting a single electron transfer step, we expect the rate-determining step to be a reductive coupling (i.e., dimerization) step of adsorbed CO intermediates, predicted from theory and carbon monoxide reduction experiments on copper (43, 49–51):



On the other hand, *n*-PrOH exhibits a different slope, suggesting a distinct rate-determining step from that of C₂ products. Estimated value is rather close to that observed for CH₄ on copper foil (86 mV/dec) (38). In addition, it has been reported that *n*-PrOH formation only occurs when reactants include both CO (carbon monoxide) and C₂H₄, while CO reduction solely leads to EtOH (28). If C₃ products followed the same pathway as C₂ products, *n*-PrOH should have been observed upon CO reduction. Instead, it may be that *n*-PrOH formation requires coupling between CO and hydrogenated carbon [e.g., carbene (*CH₂)], which is a major intermediate in the pathway to CH₄ (50). CH₄ formation activity of trans-CuEn and -CuEn 2 supports this idea as well (Figs. 3B and 4B and SI Appendix, Tables S4 and S8). In contrast to C₂H₄ and EtOH, *n*-PrOH reaches peak selectivity at a more positive potential and the potential in which *n*-PrOH FE

drops coincides well with the point where CH₄ FE starts to rise. However, it is still unclear how formation of C₃ products occur and an in-depth study of the mechanistic pathways to these products is needed.

Long-term stability was demonstrated by 10 h electrolysis of trans-CuEn 2 at -0.75 V vs. RHE (Fig. 4E). Average C₂–C₃ FE reached $\sim 50\%$ for the overall run and structural features of trans-CuEn 2 were maintained as well (SI Appendix, Fig. S26). Furthermore, stable C₂–C₃ product current density of 10 mA/cm₂^{geo} was achieved, which is potentially attractive for solar-to-fuel applications. As long-term electrolysis accumulates significant amounts of liquid products, propionaldehyde, likely to be the precursor to *n*-PrOH, was detected (SI Appendix, Fig. S27).

Stable and selective C₂–C₃ product generation achieved by the structurally transformed Cu NP ensembles presents a promising future direction to renewables-powered artificial carbon cycle. Projected solar-to-fuel efficiencies of multicarbon products (SI Appendix, Fig. S28), assuming combination of commercial Si photovoltaic devices and electrolysis configurations recently demonstrated for effective syngas formation (52, 53), are comparable or better than natural photosynthesis (e.g., 2.8% for C₂H₄). Significant mass activities are achieved as well (SI Appendix, Fig. S29), desirable in terms of cost-effectiveness, due to extremely low mass (g_{Cu}) used compared with other methods that rely on bulk Cu oxidation.

Conclusions

We have shown how an ensemble of Cu NPs can enable selective electrocatalytic conversion of CO₂ to C₂–C₃ hydrocarbons and oxygenates at significantly reduced overpotentials. Structural evolution of densely arranged Cu NPs resulted in C₂–C₃ active nanostructures and experimental investigation of the parameters affecting structural transformation and their catalytic behavior was performed. With the discovery of this active catalytic structure formed in situ, efforts in deepening the understanding of how NPs and atoms within evolve under electrically biased and chemically relevant conditions seem necessary, which will shed light on the key structural features for CO₂ conversion to multicarbon products. Furthermore, we anticipate that the unique approach of using NPs as precursors to an active nanostructured material will lead to a wide expansion of the materials library for various catalytic applications.

Methods

Copper NPs in this work are synthesized by reducing copper precursors at high temperatures with tetradecylphosphonic acid used as surface ligands. Densely packed arrangement of copper NPs on carbon support is achieved by directly loading these particles in solution to a carbon-paper electrode. Copper NPs deposited electrodes are tested for electrochemical reduction of carbon dioxide in neutral pH aqueous environments (0.1 M KHCO₃ or CsHCO₃ at 1 atm CO₂), with products measured by gas chromatography and NMR. Original copper NPs and the structures formed during electrolysis are characterized by various methods, including electron microscopy, X-ray photoelectron spectroscopy, and cyclic voltammetry. Further details of the experimental methods are provided in SI Appendix.

ACKNOWLEDGMENTS. This work was supported by Director, Office of Science, Office of Basic Energy Sciences, Chemical Sciences, Geosciences, & Biosciences Division, of the US Department of Energy under Contract DE-AC02-05CH11231, FWP CH030201 (Catalysis Research Program). Transmission electron microscopy, scanning electron microscopy, and X-ray photoelectron spectroscopy were conducted using facilities at the National Center for Electron Microscopy and Imaging and Nanofabrication facilities at the Molecular Foundry. Work at the Molecular Foundry was supported by the Office of Science, Office of Basic Energy Sciences, of the US Department of Energy under Contract DE-AC02-05CH11231. This work made use of the facilities at the NMR Facility, College of Chemistry, University of California, Berkeley. Inductively coupled plasma atomic emission spectroscopy was supported by the Microanalytical Facility, College of Chemistry, University of California, Berkeley. D.K. acknowledges the support of Samsung Scholarship. C.S.K. acknowledges support by the Alexander von Humboldt Foundation.

1. EIA (2016) *International Energy Outlook 2016* (US Energy Information Administration, Washington, DC).
2. Lewis NS (2016) Research opportunities to advance solar energy utilization. *Science* 351:aad1920.
3. Liu C, Colón BC, Ziesack M, Silver PA, Nocera DG (2016) Water splitting-biosynthetic system with CO₂ reduction efficiencies exceeding photosynthesis. *Science* 352:1210–1213.
4. Luo J, et al. (2014) Water photolysis at 12.3% efficiency via perovskite photovoltaics and Earth-abundant catalysts. *Science* 345:1593–1596.
5. Kim D, Sakimoto KK, Hong D, Yang P (2015) Artificial photosynthesis for sustainable fuel and chemical production. *Angew Chem Int Ed Engl* 54:3259–3266.
6. Vesborg PCK, Seger B, Chorkendorff I (2015) Recent development in hydrogen evolution reaction catalysts and their practical implementation. *J Phys Chem Lett* 6:951–957.
7. Luc W, et al. (2017) Ag-Sn bimetallic catalyst with a core-shell structure for CO₂ reduction. *J Am Chem Soc* 139:1885–1893.
8. Wang Z, Yang G, Zhang Z, Jin M, Yin Y (2016) Selectivity on etching: Creation of high-energy facets on copper nanocrystals for CO₂ electrochemical reduction. *ACS Nano* 10:4559–4564.
9. Weng Z, et al. (2016) Electrochemical CO₂ reduction to hydrocarbons on a heterogeneous molecular Cu catalyst in aqueous solution. *J Am Chem Soc* 138:8076–8079.
10. Hall AS, Yoon Y, Wuttig A, Surendranath Y (2015) Mesoscale-induced selectivity in CO₂ reduction catalysis. *J Am Chem Soc* 137:14834–14837.
11. Asadi M, et al. (2016) Nanostructured transition metal dithiocarbamate electrocatalysts for CO₂ reduction in ionic liquid. *Science* 353:467–470.
12. Zhu W, et al. (2014) Active and selective conversion of CO₂ to CO on ultrathin Au nanowires. *J Am Chem Soc* 136:16132–16135.
13. Chen Y, Li CW, Kanan MW (2012) Aqueous CO₂ reduction at very low overpotential on oxide-derived Au nanoparticles. *J Am Chem Soc* 134:19969–19972.
14. Gao S, et al. (2016) Partially oxidized atomic cobalt layers for carbon dioxide electroreduction to liquid fuel. *Nature* 529:68–71.
15. Liu M, et al. (2016) Enhanced electrocatalytic CO₂ reduction via field-induced reagent concentration. *Nature* 537:382–386.
16. Kim D, Resasco J, Yu Y, Asiri AM, Yang P (2014) Synergistic geometric and electronic effects for electrochemical reduction of carbon dioxide using gold-copper bimetallic nanoparticles. *Nat Commun* 5:4948.
17. Hori Y (2008) Electrochemical CO₂ reduction on metal electrodes. *Modern Aspects of Electrochemistry* (Springer, New York), pp 89–189.
18. Kuhl KP, Cave ER, Abram DN, Jaramillo TF (2012) New insights into the electrochemical reduction of carbon dioxide on metallic copper surfaces. *Energy Environ Sci* 5:7050.
19. Kas R, et al. (2014) Electrochemical CO₂ reduction on Cu₂O-derived copper nanoparticles: Controlling the catalytic selectivity of hydrocarbons. *Phys Chem Chem Phys* 16:12194–12201.
20. Chen CS, Wan JH, Yeo BS (2015) Electrochemical reduction of carbon dioxide to ethane using nanostructured Cu₂O-derived copper catalyst and palladium(II) chloride. *J Phys Chem C* 119:26875–26882.
21. Kim D, et al. (2015) Insights into an autonomously formed oxygen-evacuated Cu₂O electrode for the selective production of C₂H₄ from CO₂. *Phys Chem Chem Phys* 17:824–830.
22. Chen CS, et al. (2015) Stable and selective electrochemical reduction of carbon dioxide to ethylene on copper mesocrystals. *Catal Sci Technol* 5:161–168.
23. Lee S, Kim D, Lee J (2015) Electrocatalytic production of C₃-C₄ compounds by conversion of CO₂ on a chloride-induced bi-phasic Cu₂O-Cu catalyst. *Angew Chem Int Ed Engl* 54:14701–14705.
24. Dutta A, Rahaman M, Luedi NC, Mohos M, Broekmann P (2016) Morphology matters: Tuning the product distribution of CO₂ electroreduction on oxide-derived Cu foam catalysts. *ACS Catal* 6:3804–3814.
25. Kwon Y, Lum Y, Clark EL, Ager JW, Bell AT (2016) CO₂ electroreduction with enhanced ethylene and ethanol selectivity by nanostructuring polycrystalline copper. *ChemElectroChem* 3:1012–1019.
26. Loidice A, et al. (2016) Tailoring copper nanocrystals towards C₂ products in electrochemical CO₂ reduction. *Angew Chem Int Ed Engl* 55:5789–5792.
27. Ren D, et al. (2015) Selective electrochemical reduction of carbon dioxide to ethylene and ethanol on copper(I) oxide catalysts. *ACS Catal* 5:2814–2821.
28. Ren D, Wong NT, Handoko AD, Huang Y, Yeo BS (2016) Mechanistic insights into the enhanced activity and stability of agglomerated Cu nanocrystals for the electrochemical reduction of carbon dioxide to n-propanol. *J Phys Chem Lett* 7:20–24.
29. Mistry H, et al. (2016) Highly selective plasma-activated copper catalysts for carbon dioxide reduction to ethylene. *Nat Commun* 7:12123.
30. Handoko AD, et al. (2016) Mechanistic insights into the selective electroreduction of carbon dioxide to ethylene on Cu₂O-derived copper catalysts. *J Phys Chem C* 120:20058–20067.
31. Song Y, et al. (2016) High-selectivity electrochemical conversion of CO₂ to ethanol using a copper nanoparticle/N-doped graphene electrode. *ChemistrySelect* 1:6055–6061.
32. Roberts FS, Kuhl KP, Nilsson A (2015) High selectivity for ethylene from carbon dioxide reduction over copper nanocube electrocatalysts. *Angew Chem Int Ed Engl* 54:5179–5182.
33. Ren D, Ang BS-H, Yeo BS (2016) Tuning the selectivity of carbon dioxide electroreduction toward ethanol on oxide-derived Cu₂Zn catalysts. *ACS Catal* 6:8239–8247.
34. Gao D, et al. (2017) Plasma-activated copper nanocube catalysts for efficient carbon dioxide electroreduction to hydrocarbons and alcohols. *ACS Nano* 11:4825–4831.
35. Hori Y, Takahashi I, Koga O, Hoshi N (2003) Electrochemical reduction of carbon dioxide at various series of copper single crystal electrodes. *J Mol Catal Chem* 199:39–47.
36. Li CW, Ciston J, Kanan MW (2014) Electroreduction of carbon monoxide to liquid fuel on oxide-derived nanocrystalline copper. *Nature* 508:504–507.
37. Hoang TTH, Ma S, Gold JJ, Kenis PJA, Gewirth AA (2017) Nanoporous copper films by additive-controlled electrodeposition: CO₂ reduction catalysis. *ACS Catal* 7:3313–3321.
38. Manthiram K, Beberwyck BJ, Alivisatos AP (2014) Enhanced electrochemical methanation of carbon dioxide with a dispersible nanoscale copper catalyst. *J Am Chem Soc* 136:13319–13325.
39. Kim Y-G, Javier A, Baricuatro JH, Soriaga MP (2016) Regulating the product distribution of CO reduction by the atomic-level structural modification of the Cu electrode surface. *Electrocatalysis* 7:391–399.
40. Kim Y-G, et al. (2016) Surface reconstruction of pure-Cu single-crystal electrodes under CO-reduction potentials in alkaline solutions: A study by serial ECSTM-DEMS. *J Electroanal Chem* 780:290–295.
41. Eilert A, et al. (2017) Subsurface oxygen in oxide-derived copper electrocatalysts for carbon dioxide reduction. *J Phys Chem Lett* 8:285–290.
42. Mistry H, et al. (2016) Tuning catalytic selectivity at the mesoscale via interparticle interactions. *ACS Catal* 6:1075–1080.
43. Varela AS, Kroschel M, Reier T, Strasser P (2016) Controlling the selectivity of CO₂ electroreduction on copper: The effect of the electrolyte concentration and the importance of the local pH. *Catal Today* 260:8–13.
44. Kas R, Kortlever R, Yilmaz H, Koper MTM, Mul G (2015) Manipulating the hydrocarbon selectivity of copper nanoparticles in CO₂ electroreduction by process conditions. *ChemElectroChem* 2:354–358.
45. Ma S, et al. (2016) One-step electrosynthesis of ethylene and ethanol from CO₂ in an alkaline electrolyzer. *J Power Sources* 301:219–228.
46. Wu J, et al. (2016) A metal-free electrocatalyst for carbon dioxide reduction to multi-carbon hydrocarbons and oxygenates. *Nat Commun* 7:13869.
47. Singh MR, Kwon Y, Lum Y, Ager JW, 3rd, Bell AT (2016) Hydrolysis of electrolyte cations enhances the electrochemical reduction of CO₂ over Ag and Cu. *J Am Chem Soc* 138:13006–13012.
48. Huang Y, Handoko AD, Hirunsit P, Yeo BS (2017) Electrochemical reduction of CO₂ using copper single-crystal surfaces: Effects of CO* coverage on the selective formation of ethylene. *ACS Catal* 7:1749–1756.
49. Calle-Vallejo F, Koper MTM (2013) Theoretical considerations on the electroreduction of CO to C₂ species on Cu(100) electrodes. *Angew Chem Int Ed Engl* 52:7282–7285.
50. Kortlever R, Shen J, Schouten KJP, Calle-Vallejo F, Koper MTM (2015) Catalysts and reaction pathways for the electrochemical reduction of carbon dioxide. *J Phys Chem Lett* 6:4073–4082.
51. Pérez-Gallent E, Figueiredo MC, Calle-Vallejo F, Koper MTM (2017) Spectroscopic observation of a hydrogenated CO dimer intermediate during CO reduction on Cu(100) electrodes. *Angew Chem Int Ed Engl* 56:3621–3624.
52. Vermaas DA, Smith WA (2016) Synergistic electrochemical CO₂ reduction and water oxidation with a bipolar membrane. *ACS Energy Lett* 1:1143–1148.
53. Li YC, et al. (2016) Electrolysis of CO₂ to syngas in bipolar membrane-based electrochemical cells. *ACS Energy Lett* 1:1149–1153.